Hindawi
Advances in Materials Science and Engineering
Volume 2018, Article ID 1617280, 10 pages
https://doi.org/10.1155/2018/1617280

Research Article

Effect of Metallic Inclusions on the Compressive Strength of Cement-Based Materials

Tomáš Ficker

Faculty of Civil Engineering, Brno University of Technology, CZ-602 00 Brno, Czech Republic

Correspondence should be addressed to Tomáš Ficker; tftf@seznam.cz

Received 28 August 2018; Revised 15 October 2018; Accepted 1 November 2018; Published 26 December 2018

Academic Editor: Antonio Caggiano

In the concrete foundations, materials come into contact with bedrocks. The surfaces of bedrocks are often covered by sharp protrusions called asperities. Although geotechnical engineers have developed a reliable theory for assessing the mechanical stability of rocky terrains, the stability of transition zones between concrete and sharp asperities remains unsolved. Due to the large pressures that exist in these transition zones, the invasive influence of sharp asperities on the integrity of the concrete raises a question about possible changes of the mechanical properties of concrete materials used in foundations. These circumstances have inspired experiments in which metallic needles of various lengths have been embedded into cement-based materials to assess the influence of the needles on the compressive strength. This influence has been quantified, and the critical limits identifying the changes of material integrity have been determined. It has been conjectured that sharp rock asperities or needle-like rods of steel reinforcement in concrete may cause similar changes of material integrity as the metallic needles used in the experiments performed.

1. Introduction

In concrete research, there is a continuous interest in mechanical processes acting in the transition zones between hydrated cement matrices and aggregates [1–6]. The aggregates (sand grains and gravels) in the cement matrix (sometimes called the cement stone) play the role of fillers that do not usually increase the compressive strength of the cement-based materials, although high-quality aggregates (e.g., granite, basalt, and gneiss) very often show higher compressive strength than the cement stone itself. The reason is the imperfect transition zones between aggregates and cement stone. These imperfect zones represent critical regions (interfaces) in which microcracks often initiate. Such structural perturbations may finally lead to fatal failure, i.e., complete breakdown of the structure, if the material is faced with a higher stress. As a consequence, a lower compressive strength of these composite materials may be observed when compared with cement stone, which is a substance similar to hydrated cement paste.

Transition zones in concrete exist not only near to aggregate particles but also near to the steel reinforcement bars. Another example of the transition zone is the interface between the cement stone and rock protrusions (large asperities) in foundations. Figure 1 shows a scheme of a pillar foundation along with the photograph of the real situation. The pillar construction consists of several parts. Part B represents a leveling layer usually made of plain concrete that fills the rock irregularities (sharp asperities) that were formed during excavation work. The leveling layer B is not usually too thick, and thus the asperity layer may often occupy a considerable portion of the volume of the leveling layer. The heights of asperities may sometimes compete with the height of the leveling concrete layer. So it is not surprising that the ratio between the height of some highest asperities and the height of the leveling layer (A/B) may reach even more than 30%. Part C represents the base of the pillar, and D is the main body of the pillar. Parts C and D are made of reinforced concrete, whereas B is of plain concrete. The height E of the reinforcement approaches the height D of the pillar itself, so that the height ratio E/D may often exceed ~80%. Each part of the pillar is made subsequently after hardening of the preceding part, i.e., each part may be investigated separately as an element that is loaded individually by forces exerted by higher parts

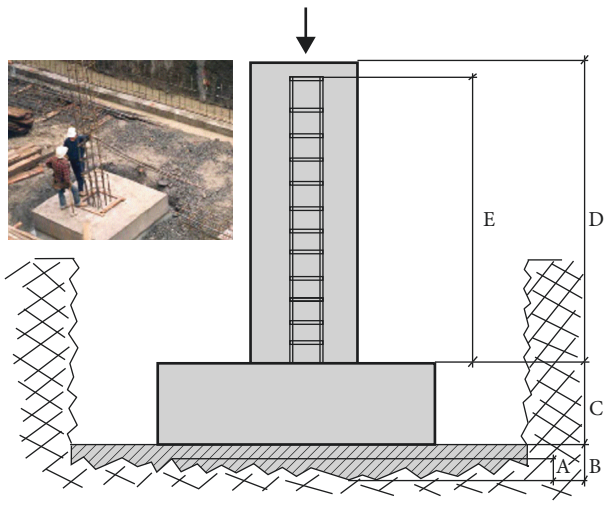

Figure 1: A scheme of pillar construction combined with the photo of the real situation.

of the construction. This especially concerns the lowest part B, called the leveling layer, since the asperities and their transition zones could introduce undesirable perturbations inside the volume of the leveling layer.

There is no reason to suppose that the transition zones accompanying the rock asperities and the metallic reinforcement behave very differently from the transition zones of gravel aggregates. All these zones may introduce certain structural imperfections that may influence the compressive strength in some cases. The sharp peaks of asperities in foundations and the steel reinforcement bars in fact represent needle-like perturbations in cement-based materials. Yet, there is a certain specificity of the transition zones bridging rock asperities and cement stone. The cement stone does not fully integrate rock asperities into its volume in contrast to the steel reinforcement bars that are fully integrated. The cement stone only touches the asperity surfaces, and the stability of such interface is prevalently determined by the mechanical wedging of both these materials.

When mechanical stability of concrete foundations in rocky terrains is explored, two aspects should be taken into account, namely, the stability of the asperity-concrete interface and the stability of rocky terrain itself.

The stability of asperity-concrete interface is determined by the mechanical wedging of asperities with concrete. The strength of this wedging depends on the asperity roughness, their mechanical strength, and the strength of concrete itself. For this reason, not only the studies of various aspects of compressive and tensile strength of concrete materials have been accomplished in our laboratory [7–9] but also the asperity roughness has been the subject of our interest in recent times [10–12].

In the geotechnical literature, there is also a continuous interest in strength properties of rock-concrete interfaces. Recently, the rock-concrete interface has been investigated by using bimaterial disks exposed to Brazilian tests [13]. These authors have identified three typical fracture patterns: interface fracture, tensile fracture, and their combination. Numerical simulations of shearing of unbounded rock-concrete planar and saw-tooth triangular joints have been realized using the shear box genesis approach. The results of these simulations have indicated that the used approach reproduces suitably the shear experimental data [14]. Rock-concrete joints with various roughness profiles have been subjected to three-point bending and four-point shear tests to investigate the propagation of interfacial cracks. The results have documented that, on the basis of the known initial fracture toughnesses of the rock, the concrete, and the rock-concrete interface, it is possible to predict the propagation of interfacial cracks in these materials and their interface [15–18]. New failure criteria for the rock, concrete, and their joints have been proposed [19, 20]. A model describing the rock deformation occurring during shearing within the rock-concrete assembly has been presented [21]. Various failure mechanisms of concrete retaining structures situated on rock foundations have been studied and shown that sliding is possible only when weakened subhorizontal surfaces with low shear parameters are present near the interface between the structure and foundation [22, 23]. The experimental study of the shear behavior of rock-concrete joints with roughness in the idealized forms of regular and irregular triangles has been performed and shown that the irregular joints have evidenced a much greater relative ductility than the regular joints [24]. A greater increase in the fracture toughness with shear loading has been observed with rock-concrete joints [25]. Shear tests have been performed with planar rock-concrete interfaces to investigate the influences of interface roughness on shear strength [26, 27].

From this overview of published results, it is clear that the research of the strength properties of rock-concrete interfaces is solely focused on shearing phenomena occurring between these two materials. Shear strength of these interfaces is predominantly investigated but practically nothing is known about the possible acting of asperities on the compressive strength of concrete materials inside foundations. The present paper is devoted just to this topic.

As the stability of the bedrock is concerned, it should be mentioned that rocky massive often consists of layers that are also mutually jointed by asperity wedging. The rock joints usually form volume networks in rock masses. An example of such a network of rock joints is shown in Figure 2. The shear strength τ of slopes consisting of rock joints may be estimated, e.g., by the empirical formula introduced by Barton [28] and Barton and Choubey [29]:

$$\tau = \sigma_n \tan\left[\mathrm{JRC}\cdot\log_{10}\left(\frac{\mathrm{JCS}}{\sigma_n}\right)+\alpha_{\max}\right], \quad (1)$$

where σ_n is the normal effective stress, JRC represents the joint roughness coefficient, JCS is the compressive strength of the joint walls, and $\alpha_{\max}$ represents a critical angle for plane joints with smooth surfaces (without asperities).

When the mechanical stability of transition zones between concrete and bedrock is considered, a question arises, namely, whether the invasive acting of sharp asperities on

Figure 2: The network of rock joints uncovered as a result of excavation work at lime quarry Hády near to the city of Brno in the Czech Republic.

concrete structure may modify the compressive strength of this material. There are no theoretical and experimental studies that would answer this question. Practitioners in geotechnics and in civil engineering usually assume a priori that asperities cannot significantly influence the mechanical properties of concrete materials. However, this question deserves attention and thorough examination at least within a model situation in which asperities could be simulated by sharp metallic needles embedded in the base of concrete specimens that would experience compressive stress.

The present contribution examines such situations. The samples made of cement-based materials with embedded metallic needles are subjected to compressive tests to verify the mechanical integrity of these materials. This contribution represents a first attempt to answer the question about the possible invasive acting of asperity-like needles in concrete materials.

2. Specimens Made of Ordinary Portland Cement Paste

It is necessary to answer the basic question whether the invasive action of small needles can modify the compressive strength of cement-based materials. For this purpose, 50 specimens (3 cm × 3 cm × 3 cm) of hydrated ordinary Portland cement paste (water-to-cement ratio = 0.3 by weight) were prepared in normal laboratory conditions. They were divided into 5 groups. Four groups contained specimens with embedded steel needles of different lengths (2 mm, 4 mm, 7 mm, and 10 mm) while the fifth group consisted of needleless specimens. After 28 days of hydration (20°C, 100% RH), the specimens were subjected to compressive tests (loading rate 0.2 MPa/s), and the resulting values were averaged within each group of specimens. Although the European standard (EN 12390-3) suggests using the loading rate of 0.6 MPa/s for compressive tests, we used a lower loading rate of 0.2 MPa/s to better satisfy the condition of static loading. In spite of the fact that the stress-controlled rate of compressive tests does not usually enable observation of the postpeak behavior of specimens, these tests make it possible to obtain the peak stress that represents the sought compressive strength. Each group of specimens consisted of 10 specimens which enabled calculation of the statistical uncertainty of the resulting compressive strength. Statistical errors were plotted as error bars in the graphs discussed in the next section. All specimens successfully passed the destructive compressive tests up to complete failure. Several such specimens are shown in Figure 3.

Figure 4 shows a microscopic three-dimensional detail of the transition zone between the cement paste and the steel needle. This figure illustrates topographical irregularities which appear in a usual transition zone. The three-dimensional projections have been performed by means of 3,937 confocal snaps made by the camera of the laser confocal microscope Olympus Lext 3100.

2.1. Experiments with Ordinary Portland Cement Paste. The averaged values of compressive strength of the tested specimens made of ordinary Portland cement paste have been plotted against the relative needle lengths ρ (Figure 5):

$$\rho = \frac{h}{H} \times 100\% = \frac{\text{needle length}}{\text{sample height}} \times 100\%. \tag{2}$$

The experimental data in Figure 5 indicate a clear dependence of the compressive strength on the lengths of the needles. An exponential function f_c,

$$f_c = f_o \exp\left(-\frac{\rho}{\rho_o}\right) + f_1, \tag{3}$$

has been fitted to the data in Figure 5, and the following optimized parameters have been obtained:

$$\begin{aligned} f_o &= 645.972\,\text{MPa}, \\ \rho_o &= 2.356\%, \\ f_1 &= 63.493\,\text{MPa}. \end{aligned} \tag{4}$$

The high absolute value of the computed correlation coefficient ~0.999 confirms that the functional type of the fitting function f_c has been chosen suitably.

The decreasing behavior of the compressive strength of the tested specimens in Figure 5 looks reasonable since longer needles in the specimens may introduce larger perturbations in the material and thus the compressive strength diminishes. However, when the values of the compressive strength are compared to the strength of the needleless specimens (the dashed horizontal line in Figure 5), it becomes evident that some needles reduce whereas others increase the compressive strength of this material. There is a certain crossing point determined by the strength curves of the needle specimens and the specimens without needles. The crossing point determines a limiting relative needle length. Below this point, the short needles increase the strength, whereas above it the longer needles decrease the strength. The critical value of the relative length belonging to the crossing point amounts to 14.28%. This means that the needles shorter than 14.28% of the specimen height may contribute to a better compressive strength of the hydrated cement paste. Such short needles fastened on the steel bases (Figure 3) introduce only negligible perturbations in the material and act as a steel reinforcement of the lower parts of the specimens.

Figure 3: Hydrated cement paste specimens containing steel needles after the final destructive tests.

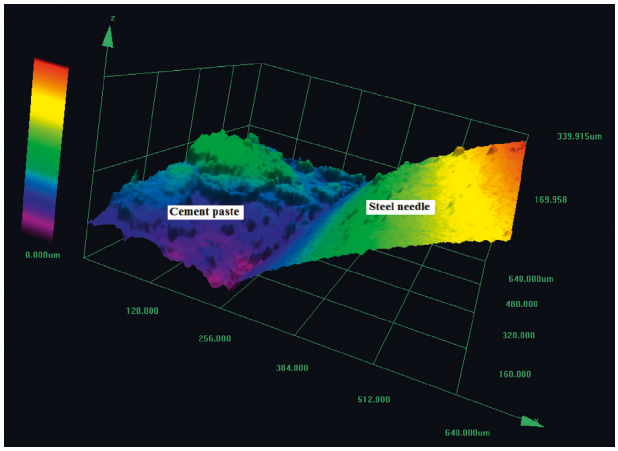

Figure 4: Microscopic three-dimensional topography of the transition zone between cement paste and the steel needle. The laser confocal microscope Olympus Lext 3100 has been used. The format of the image: 640 μm × 640 μm, 1024 pixels × 1024 pixels, vertical step $\Delta z = 0.09\,\mu$m, total height 334 μm, and magnification 20x.

The longer needles that encompass more than 15% of the specimen height may introduce such large perturbations in the hydrated cement paste that this material inevitably lowers its strength. The mentioned lowering of compressive strength does not fall to zero value but it approaches a figure close to $f_1 \approx 63.493$ MPa. This represents a decrease of 1.5 MPa (2.3%) relative to the compressive strength of the unperturbed needleless material. Although the drop of 2.3% might seem to be close to material variability, the error bars shown in Figure 5 do not support such an interpretation. In addition, the 16 MPa increase of the compressive strength caused by short needles with relative length $\rho \approx 8.5\%$ represents 24.6% increase owing to the compressive strength of the unperturbed needleless specimens, and such a large increase cannot with certainty be interpreted as the consequence of material variability.

The experiments with hydrated ordinary Portland cement paste showed that the presence of steel needles of various lengths in the volume of this material causes changes of compressive strength. When short thin steel needles ($8.5\% < \rho < 15\%$) were embedded into the volume of the specimens, the compressive strength was higher

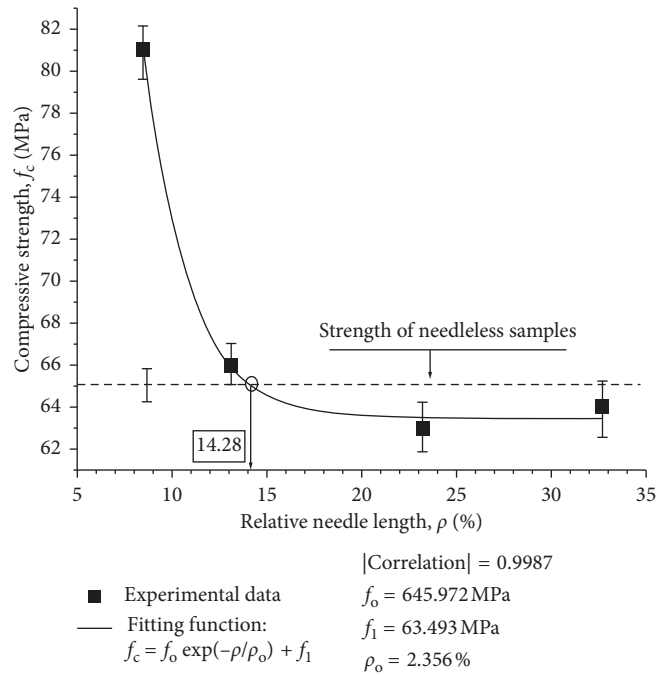

Figure 5: Compressive strength of hydrated ordinary Portland cement paste with embedded steel needles of various lengths.

than that of needleless specimens, whereas longer needles ($\rho > 15\%$) decreased the strength under the value of needleless specimens.

This surprising behavior of cement paste raised a question whether similar behavior can also be expected with other cement-based materials, e.g., with cement mortars. For this reason, a new series of larger specimens made of cement mortars (plain "concretes" with fine aggregates) were prepared to study strength changes caused by the needles.

3. Specimens Made of Cement Mortar

To simulate the action of sharp needles on the compressive strength of cement mortar, a series of specimens containing steel needles of various lengths were prepared. The cement mortar was mixed from sand with grains 0.1–0.4 mm and cement Cem I 42.5R produced in the Czech Republic. The water-to-cement-to-sand ratio was 1 : 1.943 : 7.773 by weight, i.e., the water-to-cement ratio was 0.515 by weight. Forty-eight specimens (10 cm × 10 cm × 10 cm) were molded under normal laboratory conditions. They were divided into 8 groups, each of which contained 6 specimens. Seven groups contained specimens with embedded steel needles of different lengths (5 mm, 7 mm, 11 mm, 19 mm, 29 mm, 40 mm, and 58 mm), while the eighth group consisted of needleless specimens. After 28 days of hydration in water (20°C), the specimens were subjected to compressive tests (loading rate 0.6 MPa/s), and the resulting values were averaged within each group of specimens. All the specimens successfully passed the destructive compressive tests up to complete failure. For illustration, three such specimens are shown in Figure 6 along with the steel needles.

Figure 6: Cement mortar specimens containing steel needles after the final destructive tests.

3.1. Experiments with Specimens Made of Cement Mortar. Some preliminary results concerning experiments with cement mortars were presented in the form of the conference contribution [12] but the present study of cement mortars brings a more extensive and deeper research of the studied phenomenon.

The averaged values of compressive strength of the eight investigated groups of specimens are shown in Figure 7. The same coordinate system has been used as with the cement paste, i.e., the graph of the function $f_c(\rho)$ has been plotted.

By comparing Figures 5 and 7, it is observed that the behavior of the compressive strength of cement mortar and cement paste specimens is similar. However, the larger specimens of cement mortar have enabled to investigate a new region $\rho \in (0, 10)\%$, where the curve of compressive strength has showed an increasing tendency. The small samples of cement paste (3 cm × 3 cm × 3 cm) do not show such a region since the corresponding data belonging to the interval $\rho \in (0, 10)\%$ have not been measured in this domain due to the extremely short length of needles ($l < 1$ mm). Nevertheless, both the curves in Figures 5 and 7 show a decreasing sequence in the domain of larger needles $\rho > 10\%$. The compressive strength of the cement mortar is shifted towards lower values as compared with the hydrated cement paste because of the different water-to-cement ratios. The water-to-cement ratio of cement paste is 0.3 but the ratio of cement mortar is 0.515, i.e., almost two times higher, and this inevitably results in lower compressive strength of the mortar.

A detailed analysis of the graph in Figure 7 makes it possible to distinguish further characteristic features of the investigated phenomenon. The decrease of strength of cement mortar specimens is very rapid at first ($\rho \in (10\%, 20\%)$) but for quite large needles $\rho > 20\%$, the decrease of compressive strength is considerably reduced. In addition, the overall behavior of compressive strength may be characterized by two critical points. The first of them represents a critical needle length at which the specimens show the highest value of strength, i.e., $\rho_1 \approx 10\%$. The second critical point $\rho_2 \approx 30\%$ is specified by the crossing of the graph of compressive strength with the horizontal dashed line which represents the compressive strength of the needleless mortar. To the left of the second critical point $\rho_2 \approx 30\%$, there are specimens showing higher strength, whereas to the right the specimens show lower strength as compared with the normal needleless cement mortar.

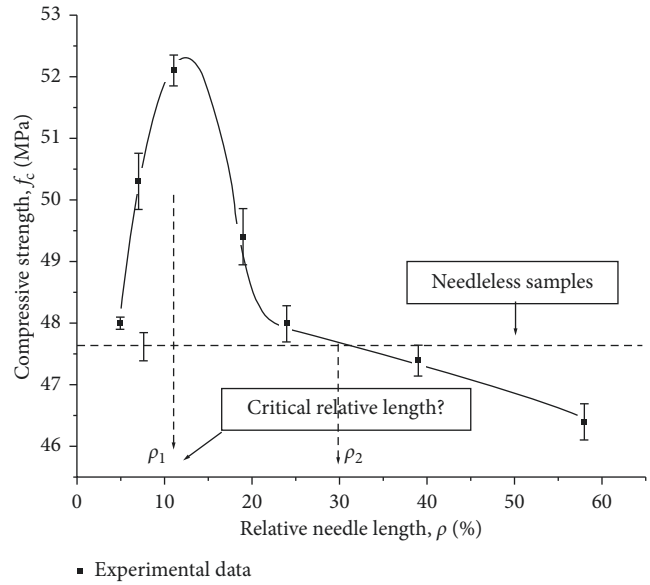

Figure 7: Compressive strength of cement mortar with embedded steel needles of various lengths.

When looking for an adequate explanation of the investigated phenomenon, it is necessary to consider the role of the needle length. It is observed that the short needles strengthen the cement mortar, whereas the longer needles reduce its compressive strength. The shorter needles may act as a certain type of reinforcement in the lower parts of the specimens. The longer needles may represent larger perturbations in the mortar specimens and as such they weaken the structure rather than reinforcing it.

Since the decreasing sequences $\rho > 10\%$ of the strength curves visible in Figures 5 and 7 seem to be of the same functional type, the former fitting function specified by equation (3) has also been used for cement mortar (naturally, the coefficients f_o, ρ_o, and f_1 resulted from the fitting procedure applied to mortar data assume different values in comparison with the fitting coefficients of cement paste):

$$f_c = f_o \exp\left(-\frac{\rho}{\rho_o}\right) + f_1, \quad \rho > \rho_1,$$

$$\rho = \frac{h}{H} \times 100\%, \tag{5}$$

$$H = 100 \text{ mm},$$

$$\begin{aligned} f_o &= 12.843 \text{ MPa}, \\ \rho_o &= 12.985\%, \\ f_1 &= 46.403 \text{ MPa}. \end{aligned} \tag{6}$$

The symbol ρ_1 is the first critical length that has been mentioned in the foregoing paragraph and is marked in Figure 7. The resulting optimized graph of function (5) is shown in Figure 8. Again, the correlation coefficient is very high (0.990), which supports the soundness of the chosen fitting function (equation (5)). It is possible to conclude that the solid needles embedded in the volume of the cement

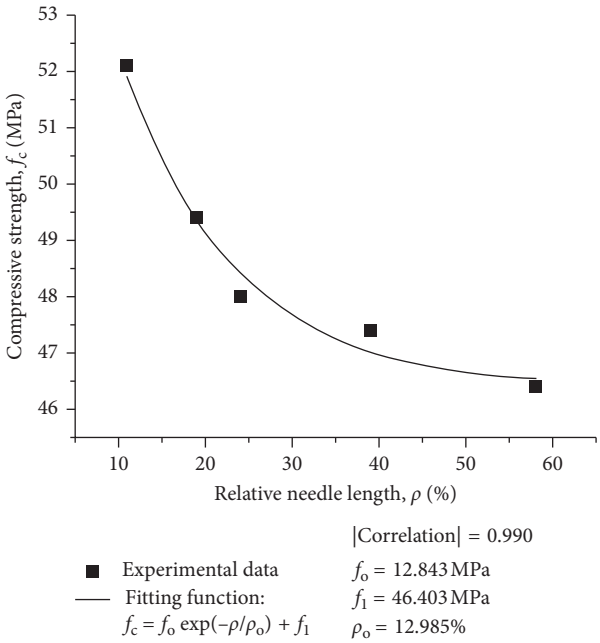

Figure 8: The decreasing sequence of compressive strength of cement mortar in dependence on relative needle length. The experimental data are identical to those presented in Figure 7.

mortar and cement paste can change the compressive strength of these materials. The strength changes are very similar in both these materials.

4. Discussion

As has been mentioned, the weakening of the structure of cement-based materials (cement paste and cement mortar) caused by the action of longer needles may be explained on the basis of the larger structural perturbations that the needles introduce in the structure. This idea is supported by the fact that the weakening of the structural strength can be described by exponential functions (3) and (5) analogously to the structural weakening caused by porosity perturbations P that are also expressed by the exponential function [30]:

$$f_c = f_o \exp\left(-\frac{P}{P_o}\right). \tag{7}$$

This functional (mathematical) analogy leads to the assumption that porosity perturbations and metallic perturbations are generically related. If this idea is correct, then there should be a chance to rewrite the exponential decrease specified by equations (3) or (5) into a functional form resembling the model of porosity perturbations (equation (7)). For this purpose, a ratio M between the perturbed volume v and the total volume V_o of the material is introduced:

$$\begin{aligned} M &= \frac{v}{V_o} \times 100\,(\%) = \frac{n \cdot h \cdot \pi \cdot r^2}{H^3} \times 100\%, \\ v &= n \cdot h \cdot \pi \cdot r^2, \\ V_o &= H^3 = 1000\,\mathrm{cm}^3, \end{aligned} \tag{8}$$

where v is the volume of metallic needles in one mortar cube, $n = 30$ is the number of needles in one mortar cube, and $r = 2$ mm is the radius of the needles used. The ratio M might be called the inclusion volume ratio of cement mortar. The inclusion volume ratio M introduced in the present paper corresponds to the well-known definition of porosity P.

The fraction ρ/ρ_o in the exponential function (5) can be replaced by the fraction M/M_o and a modified exponential function may be derived as follows:

$$\begin{aligned} \frac{\rho}{\rho_o} &= \frac{h}{\rho_o \cdot H} = \frac{n \cdot h \cdot \pi \cdot r^2}{H^3} \times \frac{H^2}{\rho_o \cdot n \cdot \pi \cdot r^2} \\ &= \frac{v}{V_o} \times \frac{H^2}{\rho_o \cdot n \cdot \pi \cdot r^2} = \frac{M}{M_o}, \end{aligned} \tag{9}$$

$$M_o = \frac{\rho_o \cdot n \cdot \pi \cdot r^2}{H^2} = 0.489 \approx 0.49\%, \tag{10}$$

$$f_c = f_o \exp\left(-\frac{M}{M_o}\right) + f_1, \quad \text{for } M \geq 0.38\%,$$

$$\rho > \rho_1 = \frac{h_1}{H} \Longrightarrow M > M_1 = \frac{h_1}{H} \times \frac{n \cdot \pi \cdot r^2}{H^2} \times 100\% \approx 0.38\%. \tag{11}$$

If all these considerations and derivations are correct, then the fit of the exponential pattern (11) to the cement mortar data should result in the same values of f_o and f_1 as in equation (6), and the parameter M_o should be equal to 0.49 as in equation (10). The results of the fitting procedure are presented in Figure 9. The procedure of least squares has provided the following parameters:

$$\begin{aligned} f_o &= 12.843\,\mathrm{MPa}, \\ M_o &= 0.495\% \approx 0.49\%, \\ f_1 &= 46.403\,\mathrm{MPa}, \end{aligned} \tag{12}$$

which are in good agreement with equations (6) and (10). The high correlation coefficient 0.990 has again confirmed the soundness of the fitting procedure.

Finally, it should be mentioned that there are some differences between the functions (7) and (11). First of all, the concept of inclusion volume ratio M in contrast to porosity P is restricted by a numerical extent. For example, f_c in equation (11) cannot approach a real value f_o of the needleless cubes since function (11) describes only the region to the right of the first critical point $\rho > \rho_1$, and for the left interval $\rho < \rho_1$, this pattern is inapplicable. In reality, M cannot go to "infinity" since the length of the needles is restricted by the size of the cubes H. Thus, the maximum value of M is restricted by the maximum length of the needles ($h_{max} = H$) and their numbers n (in our case $n = 30$), i.e., $M_{max} = (n \cdot \pi \cdot r^2/H^2) \times 100\% = 3.77\%$. Therefore, the following relation has to be fulfilled for maximum M_{max}:

$$f_c(M_{max}) \approx \lim_{M \longrightarrow \infty} f_c(M) = f_1. \tag{13}$$

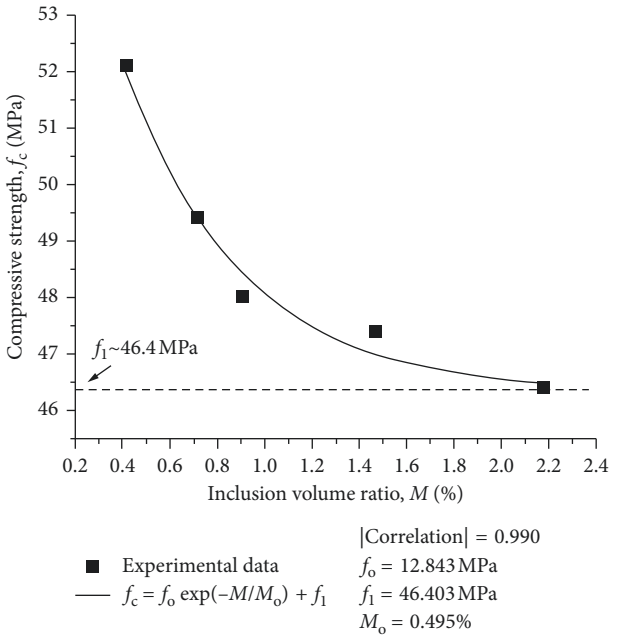

Figure 9: The decreasing sequence of compressive strength of cement mortar in dependence on inclusion volume ratio. The experimental data are identical to those presented in Figures 7 and 8.

This can be easily verified by inserting $M_{max} = 3.77\%$ into equation (11). The resulting value of compressive strength $f_c(M_{max}) = 46.409$ MPa corresponds almost exactly to the optimized value $f_1 = 46.403$ MPa.

All these results support our hypothesis about the analogy between the relative content of inclusions M and the porosity P. Yet, the aforementioned experimental procedures showing the responsibility of transition zones for lowering the compressive strength would rather be incomplete if the influence of the areal extent of the zones on the compressive strength were not explored. The next paragraph will shed light on the problem and will bring a desirable rationalization of the studied phenomenon.

First of all, it is evident that the thicknesses of all the transition zones between the metallic needles and the cement stone are nearly identical because all the metallic needles have the same shapes and are made of the same material, and the cement stones have been prepared with the same cement material and have hydrated under the same conditions. But the total area of the jointed surfaces (metal needles versus stone) extends when the lengths of the needles are enlarging. Thus, the phenomenon of lowering compressive strength should be dependent on the extending area of the interfaces between these two materials and, as a consequence, the exponential decrease of compressive strength should also be dependent on this area. Since the area of the bases of the needles is constant (i.e., $n \times 2\pi r^2$) and only the area of the side walls of the needles are extending, the relevant increasing area is given by the side envelopes of the needles, i.e., $s = n \times 2\pi rh$. A transition zone represents structural weakness in a material, and extending areas of zones are accompanied by a higher risk (higher probability) of structural collapse when the material is faced with shear stresses acting along the borders of the transition zones. Since the needles are loaded in vertical positions, their side envelopes experience shear stress. Thus, the shearing of materials along the side envelopes of the needles may be the crucial mechanism leading to perturbation of the cement stone and, as a consequence, the propagation of microcracks may be directed vertically, continuing the orientations of the needle sides as shown in Figure 10. Due to the destructive shearing along the side walls of the needles, the total critical area s may be relevant also for model considerations. If this concept is correct, the active area of zones s should be implicitly included in the formerly used inclusion volume ratio M/M_o. This is documented in the following derivation (see also equation (9)):

$$\begin{aligned}\frac{M}{M_o} &= \frac{v}{V_o} \times \frac{H^2}{\rho_o \cdot n \cdot \pi \cdot r^2} = \frac{n \cdot \pi \cdot r^2 \cdot h}{H^3} \times \frac{H^2}{\rho_o \cdot n \cdot \pi \cdot r^2} \\ &= \frac{n \cdot 2\pi \cdot r \cdot h}{6H^2} \times \frac{3H \cdot r}{\rho_o \cdot n \cdot \pi \cdot r^2} \\ &= \frac{s}{S_o} \times \frac{1}{((\rho_o \cdot n \cdot \pi \cdot r)/3H)} = \mu \times \frac{1}{\mu_o} = \frac{\mu}{\mu_o},\end{aligned} \tag{14}$$

where $S_o = 6H^2 = 0.06\ m^2$ is the constant surface area of one cube specimen (S_o serves as a reference quantity), $\mu_o = (\rho_o \cdot n \cdot \pi \cdot r)/(3H) = 8.1587\%$ is a constant quantity since H and r are also constants in our experiment, and $\mu = s/S_o$ is a relative dimensionless area of transition zones and will be called the "zone area ratio." To verify this theoretical scheme experimentally, a plot of the couples of data (μ, f_c) has been realized and the results are shown in Figure 11. Again, a decrease of compressive strength has been manifested, and the data have been fitted by the exponential function:

$$f_c = f_o \exp\left(-\frac{\mu}{\mu_o}\right) + f_1. \tag{15}$$

The fitting procedure performed by the least-squares method has yielded the following optimized numbers:

$$\begin{aligned} f_o &= 12.843\ \text{MPa}, \\ \mu_o &= 8.1586\%, \\ f_1 &= 46.403\ \text{MPa}. \end{aligned} \tag{16}$$

These numbers fully confirm the derivations presented in equation (14) and, in addition, the numerical agreement between the calculated value $\mu_o = 8.1587\%$ and the fitted value $\mu_o = 8.1586\%$ documents a full harmony between the theoretical model and the experiment. The model of shear stress acting along the side walls of the vertical needles has enabled us to correlate the compressive strength with the area of the side walls, which are actually areal borders of the transition zones. The side walls form envelopes of the "cavities" that are filled with metallic needles. Because the total area s of all the side envelopes and the total volume v of all the "cavities" in one cube specimen are tightly correlated ($v = s \times r/2$, r = const.), it should not be surprising that the

Figure 10: A microcrack propagation along the metallic needle embedded in hydrated cement paste. The crack continues the vertical direction of the needle side wall.

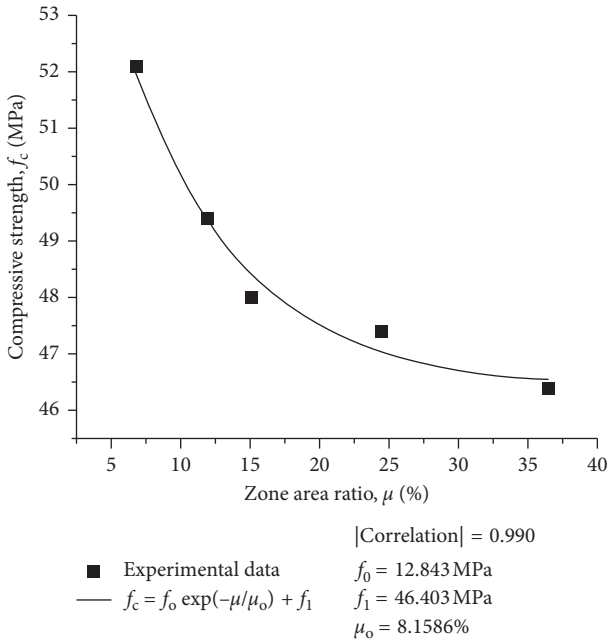

Figure 11: The decreasing sequence of compressive strength of cement mortar in dependence on zone area ratio. The experimental data are identical to those shown in Figures 7–9.

exponential decrease of compressive strength can be described by both the volume and area ratios, i.e., by the M and μ parameters, respectively:

$$\frac{\rho}{\rho_o} = \frac{M}{M_o} = \frac{\mu}{\mu_o}. \tag{17}$$

Since no chemical bonds are established between the metallic needles and cement stone, the studied phenomenon is of purely mechanical origin, and it may be hypothesized that after replacing the metallic needles by high-strength peaked asperities oriented vertically as the metallic needles, an analogous behavior of compressive strength might be observed. At least two conditions have to be fulfilled in order that a decrease of compressive strength may occur: (1) the compressive strength of the needle-like asperities should be larger than that of cement stone; (2) the relative asperity length ρ should exceed the critical limit ρ_1 that is specifically optimized for transition zones between asperities and cement stone. Condition (2) may be easily fulfilled, e.g., in the leveling concrete layers mentioned in Introduction. It is not excluded that the vertically oriented steel reinforcement bars in concrete may also be considered analogously to the vertical needles in our experiments.

One important point has not been discussed so far, namely, the effect of the "population" density of needles on the compressive strength of cement-based materials. The "population" density (σ) of needles, i.e., the number of needles per unit area, is a very important factor since it determines, together with the dimensions of the needles, the volume and area ratios, i.e., $M = v/V_o$ and $\mu = s/S_o$, respectively. By varying the population density σ of needles of constant relative height ρ, both the volume M and area μ ratios are varied accordingly. This means that volume and area parameters M and μ are of the same importance as the parameters ρ. The two parameters M and μ include the influence of both the population density σ and the relative length ρ. To obtain critical limits for parameters M and μ, it is possible to use equation (17) and previously found limits $\rho_1 \approx 10\%$ and $\rho_2 \approx 30\%$ measured at a constant population density ($\sigma = 30\,\mathrm{dm}^{-2}$):

$$\begin{aligned} M_1 &= \frac{\rho_1}{\rho_o} \times M_o = \frac{10}{12.985} \times 0.495 = 0.381\%, \\ M_2 &= \frac{\rho_2}{\rho_o} \times M_o = \frac{30}{12.985} \times 0.495 = 1.144\%, \\ \mu_1 &= \frac{\rho_1}{\rho_o} \times \mu_o = \frac{10}{12.985} \times 8.159 = 6.283\%, \\ \mu_2 &= \frac{\rho_2}{\rho_o} \times \mu_o = \frac{30}{12.985} \times 8.159 = 18.850\%. \end{aligned} \tag{18}$$

The most practical parameters seem to be the inclusion volume ratios M since they can be easily determined in practice. The first critical parameter M_1 specifies the situation at which the compressive strength reaches its maximum value high above the normal compressive strength of needleless materials, and the second parameter M_2 determines the critical point at which the compressive strength drops under the normal compressive strength of needleless materials.

The parameters $M_1 \approx 0.38\%$ and $M_2 \approx 1.14\%$ can hardly be universal for all cement-based materials since different compositions of these materials inevitably change the mechanical properties of transition zones, and thus the critical limits M_1 and M_2 may change more or less their values. Nevertheless, each of these materials will have its own characteristic values for M_1 and M_2.

5. Conclusions

On the basis of the experiments presented in this paper, several conclusions may be drawn:

(i) Short needle inclusions ($\rho < \rho_2$) whose relative volume content M in cement-based materials is

sufficiently small ($M < M_2$) do not worsen the compressive strength and may even contribute to a better material integrity.

(ii) Longer needle inclusions ($\rho > \rho_2$) with higher relative content $M > M_2$ may worsen the compressive strength of cement-based materials.

(iii) The critical parameters $\rho_{1,2}$, $M_{1,2}$, and $\mu_{1,2}$ are not universal quantities but are dependent on the type of cement-based materials and the mechanical and shape properties of the needle-like inclusions.

(iv) A hypothesis has been put forward that high-strength sharp asperities of bedrocks might act in thin concrete leveling layers similarly to needle-like inclusions. This may especially concern rock asperities composed of high-quality materials such as granite, basalt, or gneiss.

(v) There is no doubt that the steel reinforcements usually used in concrete effectively improve the values of tensile and flexural strength. However, in light of the performed experiments, it is not excluded that the steel reinforcement rods in concrete may act like the invasive steel needles modifying the compressive strength of concrete in some special cases.

Data Availability

The data which served for plotting the graphs presented in this study are available from the corresponding author upon request.

Conflicts of Interest

The author declares that there are no conflicts of interest regarding the publication of this paper.

Acknowledgments

This paper was supported by the Grant Agency of the Czech Republic under grant no. 13-03403S. The grant support had started in 2013 and finished in 2017.

References

[1] H. Jin, Y. Zhou, B. Wang, and S. Zhou, "Mesoscopic finite element modeling of concrete considering geometric boundaries of actual aggregates," *Advances in Materials Science and Engineering*, vol. 2018, Article ID 7816502, 10 pages, 2018.

[2] B. Mielniczuk, M. Jebli, F. Jamin, M. S. El Youssoufi, C. Pelissou, and Y. Monerie, "Characterization of behavior and cracking of a cement paste confined between spherical aggregate particles," *Cement and Concrete Research*, vol. 79, pp. 235–242, 2016.

[3] Y. J. Peng, H. Chu, and J. W. Pu, "Numerical simulation of recycled concrete using convex aggregate model and base force element method," *Advances in Materials Science and Engineering*, vol. 2016, Article ID 5075109, 10 pages, 2016.

[4] X. H. Wang, S. Jacobsen, J. Y. He, Z. L. Zhang, S. F. Lee, and H. L. Lein, "Application of nanoindentation testing to study of the interfacial transition zone in steel fiber reinforced mortar," *Cement and Concrete Research*, vol. 39, no. 8, pp. 701–715, 2009.

[5] K. Wu, H. Shi, L. Xu, G. Ye, and G. De Schutter, "Microstructural characterization of ITZ in blended cement concretes and its relation to transport properties," *Cement and Concrete Research*, vol. 79, pp. 243–256, 2016.

[6] G. Yue, P. Zhang, Q. Li, and Q. Li, "Performance analysis of a recycled concrete interfacial transition zone in a rapid carbonization environment," *Advances in Materials Science and Engineering*, vol. 2018, Article ID 1962457, 8 pages, 2018.

[7] T. Ficker, "Fitting function for flexural strength of cement paste," in *Proceedings of World Multidisciplinary Civil Engineering-Architecture-Urban Planning Symposium (WMCAUS)*, vol. 245, Published in Book Series: IOP Conference Series-Materials Science and Engineering, Prague, Czech Republic, June 2017.

[8] T. Ficker, "Rupture strength and irregularity of fracture surfaces," in *Proceedings of World Multidisciplinary Civil Engineering-Architecture-Urban Planning Symposium (WMCAUS)*, vol. 245, Published in Book Series: IOP Conference Series-Materials Science and Engineering, Prague, Czech Republic, June 2017.

[9] T. Ficker, "Fractal properties of joint roughness coefficients," *International Journal of Rock Mechanics and Mining Sciences*, vol. 94, pp. 27–31, 2017.

[10] O. Audy and T. Ficker, "Fractal analysis of rock joint profiles," in *Proceedings of World Multidisciplinary Civil Engineering-Architecture-Urban Planning Symposium (WMCAUS)*, vol. 245, Published in Book Series: IOP Conference Series-Materials Science and Engineering, Prague, Czech Republic, June 2017.

[11] O. Audy and T. Ficker, "Evaluation of rock joint coefficients," in *Proceedings of World Multidisciplinary Civil Engineering-Architecture-Urban Planning Symposium (WMCAUS)*, vol. 245, Published in Book Series: IOP Conference Series-Materials Science and Engineering, Prague, Czech Republic, June 2017.

[12] T. Ficker and T. Komárková, "Rock joints asperities and mechanical strength of concrete," in *Proceedings of World Multidisciplinary Civil Engineering-Architecture-Urban Planning Symposium (WMCAUS)*, vol. 245, Published in Book Series: IOP Conference Series-Materials Science and Engineering, Prague, Czech Republic, June 2017.

[13] X. Chang, J. Lu, S. Wang, and S. Wang, "Mechanical performances of rock-concrete bi-material disks under diametrical compression," *International Journal of Rock Mechanics and Mining Sciences*, vol. 104, pp. 71–77, 2018.

[14] J. G. Gutiérrez-Ch, S. Senent, S. Melentijevic, and R. Jimenez, "Distinct element method simulations of rock-concrete interfaces under different boundary conditions," *Engineering Geology*, vol. 240, pp. 123–139, 2018.

[15] W. Dong, D. Yang, B. Zhang, and Z. Wu, "Rock-concrete interfacial crack propagation under mixed mode I-II fracture," *Journal of Engineering Mechanics*, vol. 144, no. 6, article 04018039, 2018.

[16] W. Dong, D. Yang, X. Zhou, G. Kastiukas, and B. Zhang, "Experimental and numerical investigations on fracture process zone of rock-concrete interface," *Fatigue and Fracture of Engineering Materials and Structures*, vol. 40, no. 5, pp. 820–835, 2016.

[17] W. Dong, Z. Wu, X. Zhou, N. Wang, and G. Kastiukas, "An experimental study on crack propagation at rock-concrete

interface using digital image correlation technique," *Engineering Fracture Mechanics*, vol. 171, pp. 50–63, 2017.

[18] W. Dong, Z. Wu, and X. Zhou, "Fracture mechanisms of rock-concrete interface: experimental and numerical," *Journal of Engineering Mechanics*, vol. 142, no. 7, article 04016040, 2016.

[19] H. Jiang, "A failure criterion for rocks and concrete based on the Hoek-Brown criterion," *International Journal of Rock Mechanics and Mining Sciences*, vol. 95, pp. 62–72, 2017.

[20] Z. J. Yang and A. J. Deeks, "Fully-automatic modelling of cohesive crack growth using a finite element-scaled boundary finite element coupled method," *Engineering Fracture Mechanics*, vol. 74, no. 16, pp. 2547–2573, 2007.

[21] V. Andjelkovic, N. Pavlovic, Z. Lazarevic, and V. Nedovic, "Modelling of shear characteristics at the concrete-rock mass interface," *International Journal of Rock Mechanics and Mining Sciences*, vol. 76, pp. 222–236, 2015.

[22] Y. A. Fishman, "Stability of concrete retaining structures and their interface with rock foundations," *International Journal of Rock Mechanics and Mining Sciences*, vol. 46, no. 6, pp. 957–966, 2009.

[23] Y. A. Fishman, "Features of shear failure of brittle materials and concrete structures on rock foundations," *International Journal of Rock Mechanics and Mining Sciences*, vol. 45, no. 6, pp. 976–992, 2008.

[24] J. K. Kodikara and I. W. Johnston, "Shear behaviour of irregular triangular rock-concrete joints," *International Journal of Rock Mechanics and Mining Sciences and Geomechanics Abstracts*, vol. 31, no. 4, pp. 313–322, 1994.

[25] K. M. Lee and O. Buyukozturk, "Fracture analysis of mortar-aggregate interfaces in concrete," *Journal of Engineering Mechanics*, vol. 118, no. 10, pp. 2031–2047, 1992.

[26] I. W. Johnston and T. S. K. Lam, "Shear behavior of regular triangular concrete/rock joints-analysis," *Journal of Geotechnical Engineering*, vol. 115, no. 5, pp. 711–727, 1989.

[27] T. S. K. Lam and I. W. Johnston, "Shear behavior of regular triangular concrete/rock joints-evaluation," *Journal of Geotechnical Engineering*, vol. 115, no. 5, pp. 728–740, 1989.

[28] N. Barton, "Review of a new shear-strength criterion for rock joints," *Engineering Geology*, vol. 7, no. 4, pp. 287–332, 1973.

[29] N. Barton and V. Choubey, "The shear strength of rock joints in theory and practice," *Rock Mechanics Felsmechanik Mécanique des Roches*, vol. 10, no. 1, pp. 1–54, 1977.

[30] P. K. Mehta and P. J. M. Monteiro, *Concrete, Microstructure, Properties and Materials*, McGraw-Hill, New York, NY, USA, 3rd edition, 2006.